Article

Factorizing Selectivity Determinants of Inhibitor Binding toward Aldose and Aldehyde Reductases: Structural and Thermodynamic Properties of the Aldose Reductase Mutant Leu300Pro–Fidarestat Complex

Tatiana Petrova, Holger Steuber, Isabelle Hazemann, Alexandra Cousido-Siah, Andre Mitschler, Roland Chung, Mitsuru Oka, Gerhard Klebe, Ossama El-Kabbani, Andrzej Joachimiak, and Alberto Podjarny

J. Med. Chem., **2005**, 48 (18), 5659-5665• DOI: 10.1021/jm050424+ • Publication Date (Web): 05 August 2005

Articles

Factorizing Selectivity Determinants of Inhibitor Binding toward Aldose and Aldehyde Reductases: Structural and Thermodynamic Properties of the Aldose Reductase Mutant Leu300Pro−Fidarestat Complex

Tatiana Petrova,[§,||] Holger Steuber,[⊥] Isabelle Hazemann,[§] Alexandra Cousido-Siah,[§] Andre Mitschler,[§] Roland Chung,[†] Mitsuru Oka,[#] Gerhard Klebe,[⊥] Ossama El-Kabbani,[†] Andrzej Joachimiak,[‡] and Alberto Podjarny*[,§]

Laboratoire de Génomique et de Biologie Structurales, UMR 7104 du CNRS, IGBMC, 1 Rue Laurent Fries, B.P. 10142, 67404 Illkirch, France, Department of Pharmaceutical Chemistry, University of Marburg, Marbacher Weg 6, D35032 Marburg, Germany, Department of Medicinal Chemistry, Victorian College of Pharmacy, Monash University (Parkville Campus), 381 Royal Parade, Vic 3052, Australia, Sanwa Kagaku Kenkyusyo Company, Ltd., 363, Shiosaki, Hokusei-cho, Inabe-shi, Mie 511-0406, Japan, and Structural Biology Center, Biosciences Division, Argonne National Laboratory, Argonne, Illinois 60439

Received May 4, 2005

Structure of the Leu300Pro mutant of human aldose reductase (ALR2) in complex with the inhibitor fidarestat is determined. Comparison with the hALR2−fidarestat complex and the porcine aldehyde reductase (ALR1)−fidarestat complex indicates that the hydrogen bond between the Leu300 amino group of the wild-type and the exocyclic amide group of the inhibitor is the key determinant for the specificity of fidarestat for ALR2 over ALR1. Thermodynamic data also suggest an enthalpic contribution as the predominant difference in the binding energy between the aldose reductase mutant and the wild-type. An additional selectivity-determining feature is the difference in the interaction between the inhibitor and the side chain of Trp219, ordered in the present structure but disordered (corresponding Trp220) in the ALR1−fidarestat complex. Thus, the hydrogen bond (∼7 kJ/mol) corresponds to a 23-fold difference in inhibitor potency while the differences in the interactions between Trp219(ALR2) and fidarestat and between Trp220(ALR1) and fidarestat can account for an additional 10-fold difference in potency.

Introduction

Aldose reductase (ALR2, EC 1.1.1.21) is a member of the aldo−keto reductase superfamily that catalyzes the NADPH-dependent reduction of a broad range of aldehydes and ketones.[1,2] ALR2 is the first enzyme in the polyol pathway and converts glucose to sorbitol, which is subsequently transformed to fructose by sorbitol dehydrogenase. During a hyperglycemic event, the elevated glucose flux through the polyol pathway enhances ALR2 activity and has been shown to play a key role in diabetic long-term onset complications such as neuropathy and nephropathy.[3] The consequent accumulation of sorbitol in the eye is believed to be responsible for the development of glaucoma, retinopathies, and cataracts in diabetic patients.[4] Inhibition of ALR2 thus offers patients suffering from diabetes mellitus a viable therapeutic measure against the debilitating pathologies associated with chronic hyperglycemia.[5−7] While many aldose reductase inhibitors (ARIs) have been reported in the literature, adverse side effects and lack of efficacy have curtailed the prospect of many drug candidates for clinical use. Epalrestat is the only ARI that is currently marketed for treatment of diabetic neuropathy in Japan, with several other potential candidates in current clinical trials.[7−9]

It is widely believed that the unfavorable profile of many ARIs in clinical trials is due to their concurrent inhibition of the closely related aldehyde reductase (ALR1, EC 1.1.1.2),[10] which is responsible for the reduction of many aldehydes and metabolizes methyl glyoxal and 3-deoxyglucosone, which are intermediates in the formation of toxic advanced glycation end products.[1,11] ALR1 has a 65% sequence identity with ALR2 and belongs to the same aldo−keto reductase superfamily.[1] This overall sequence identity is of secondary importance, the most important are the identities and differences at the active site. Both enzymes are composed of similar α/β TIM barrels,[12] with the nicotinamide moiety of NADPH located in an active site position that allows a hydride transfer from the C-4 atom to the carbonyl group of the substrate while a proton is provided by the conserved Tyr48 residue of ALR2 (Tyr50 in ALR1).[13] Because of these structural and functional similarities, it is therefore not surprising that many ARIs inhibit ALR1 as well. The loss of ALR1 activity will ostensibly invoke significant functional ramifications. It is therefore necessary to identify any structural differences between these enzymes that may

* To whom correspondence should be addressed. Phone: +33 3 88 65 33 11. Fax: + 33 3 88 65 32 01. E-mail: podjarny@titus.u-strasbg.fr.
[§] Laboratoire de Génomique et de Biologie Structurales.
[||] Permanent address: Institute of Mathematical Problems of Biology, Russian Academy of Sciences, Pouschino, Russia.
[⊥] University of Marburg.
[†] Monash University (Parkville Campus).
[#] Sanwa Kagaku Kenkyusyo Company, Ltd.
[‡] Argonne National Laboratory.

10.1021/jm050424+ CCC: $30.25
Published on Web 08/05/2005

be exploited in the design of inhibitors that are highly selective for ALR2 over ALR1. The selectivity of an inhibitor for ALR2 is typically expressed by the activity ratio of ALR2 compared to ALR1 inhibition at a given concentration.[1]

Traditionally, ARIs emerged from two major classes, depending on whether they contain an acetic acid moiety[14] or a cyclic imide group. The latter in turn comprises hydantoin/imidazoline-2,4-dione derivatives,[15] such as fidarestat and sorbinil, or succinimide derivatives,[16] like minalrestat and AS-3201. These polar groups are usually attached to a hydrophobic ring system.[6] X-ray structures of several ALR2−inhibitor complexes showed that the polar hydantoin and carboxylate groups bind in a conserved anion-binding site adjacent to the nicotinamide ring of the coenzyme. They form hydrogen bonds with ALR2 residues Tyr48, His110 and Trp111.[12,15] Inhibitors containing either the cyclic imide or carboxylic acid anchor exhibit similar in vitro but lower in vivo activity with respect to the carboxylic acid derivatives. This observation has been attributed to the relatively lower pK_a values and accordingly their ionization at physiological pH.[17−19] Most ALR2 inhibitors are also effective against ALR1 because they bind to the enzyme in a very similar manner with the polar inhibitor moiety wedged between the nicotinamide ring and the conserved residues Tyr48, His110, and Trp79.[12,20,21] The hydrophobic ring systems of the inhibitors are bound tightly in a pocket that is adjacent to the anion-binding site. Inhibition and biochemical studies have suggested that inhibitors with different potencies for ALR1 and ALR2 are likely to interact with residues residing in the C-terminal loop,[20,22] since this portion is not conserved across members of the aldo−keto reductase superfamily.[1] Moreover, crystallographic and modeling studies of ALR1 and ALR2 in complex with inhibitors have shown that inhibitors specific to ALR2 interact with C-terminal residues by binding to the same subsite, which has been described as the "specificity" pocket.[12,15,23]

In the present study, a crystal structure was determined for the complex of a Leu300 to Pro300 (Leu300Pro) mutant of the human ALR2 holoenzyme with the bound inhibitor (2*S*,4*S*)-6-fluoro-2′,5′-dioxospiro[chroman-4,4′-imidazoline]-2-carboxamide (fidarestat). Recently, the structure of human ALR2 in complex with fidarestat has been determined (PDB code 1PWM). It has been suggested that cyclic imides cross the biological membrane as neutral species before releasing a proton and subsequently binding to the active site as an anion.[24] The hydantoin ring of fidarestat is located in the conserved anion-binding site between the nicotinamide ring of the NADPH and the active site residues Tyr48, His110, and Trp111. Its chroman ring is located within van der Waals contact distance of the side chains comprising the "specificity" pocket residues Trp20, Trp111, Phe122, and Trp219, while its exocyclic amide (carbamoyl) group forms a hydrogen bond with the main chain nitrogen of Leu300. This interaction was proposed to be the major factor for the high fidarestat affinity and selectivity advantage toward ALR2 over ALR1.[15] In an attempt to confirm this assumption, site-directed mutagenesis was carried out with the specific goal of converting Leu300 into a Pro residue, which represents the ALR1 equivalent of Pro301. Determination of the crystal structure of the corresponding mutant ternary complex will allow the direct comparison of the interaction pattern with that of the previously determined ALR2 ternary complex.[24,25] A calorimetric study will also be undertaken to investigate any changes in binding energies as a consequence of this mutation.

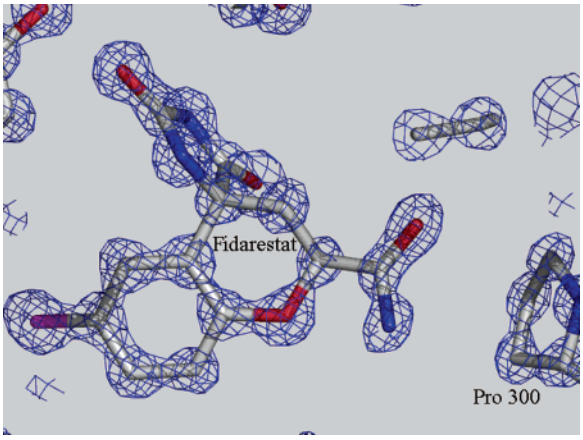

Figure 1. Electron density map $2F_o - F_c$ contoured at 2.5σ around fidarestat bound to the Leu300Pro mutant at a resolution of 1 Å.

Results and Discussion

The Leu300Pro mutant of aldose reductase was cloned, expressed, and purified as described in Materials and Methods. Cocrystals with fidarestat were prepared, and the structure was solved using molecular replacement and refined to a resolution of 1.0 Å. The mutated proline and the inhibitor appeared clearly in the electron density map (Figure 1).

Aldose reductase folds into an eight-stranded α/β barrel, with the active site located at the C-terminal end of the barrel. A total of 316 residues, $NADP^+$, fidarestat, and 588 solvent molecules constitute the final model. Multiple conformations were observed for 98 residues. In a Ramachandran plot, 90.3% of the residues (excluding Gly) are in the most favorable region and 9.7% (excluding Gly) are in the allowed region.

High-Resolution Features of the Leu300Pro ALR2−Fidarestat Complex Structure. The structure shows all the characteristic details of a high-resolution structure. In ordered regions ($B < 7$ Å^2) several hydrogen atoms are observed, attached to main chain atoms and even some of those attached to side chain atoms. These observations allow experimental determination of protonation states of some residues and the unique assignment of H-bonds.

The overall stereochemical quality of the final model was inspected using PROCHECK.[26] The average of the ω angle shows an rms deviation from the peptide bond planarity of 6.0°. This value matches a mean typically found by PROCHECK for normal proteins. Nevertheless, some significant deviations from this mean are observed. An example is the Ser76−Lys77 peptide bond (ω angle of −166.7°, a deviation of 13.3° from the standard value) where the deviation from planarity is stabilized by an H-bond between the nitrogen atom of Lys77 and the side chain oxygen atom of Ser76. The same geometry was observed in several other complexes ALR2−inhibitor, like the one with IDD594.[27] Lys77 is

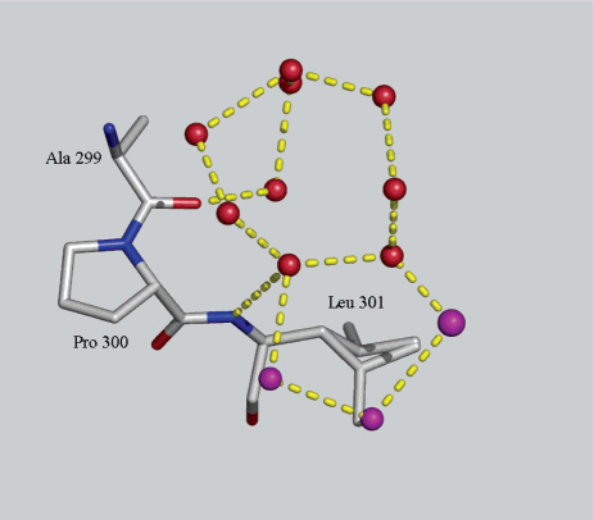

Figure 2. Water network near the mutated proline site. Waters with tetrahedral geometry are indicated by red spheres; waters with pentameric geometry are indicated by magenta spheres. Note that the pentameric network is completed with two tetrahedric waters. Hydrogen bonds are shown by dashed lines.

supposed to be involved in the enzymatic mechanism because Lys77-NZ polarizes the catalytically important hydroxyl group of Tyr48.

A characteristic of the high-resolution structure is the clear visibility of solvent at the protein surface, which represents an excellent source of information for the study of protein hydration. In the Leu300Pro ALR2−fidarestat structure, several tetrahedral arrangements and pentameric clusters of water molecules are observed. An example is shown in Figure 2, where the water network near the mutated proline is shown. One network of tetrahedrally coordinated waters is linked to O (Ala299) and N (Leu301). This network shares an edge with a pentameric polygon facing a hydrophobic region of the protein (the double conformation of Leu301). These observations are similar to those previously reported for the ALR2−IDD594 complex.[27]

Inhibitor Binding Site. The active site represents a well-ordered region as apparent from the electronic density map (Figure 1) and in agreement with low *B* factor values (~6 Å^2). The inhibitor fidarestat binds to this site, adopting an orientation very close to that observed for the complex with ALR2 wild-type.[24] The inhibitor's hydantoin moiety is placed deeply into the active site, interacting with the residues Tyr48, His110, Trp111, and the cofactor NADP$^+$. The N atom of this moiety is placed at 2.76 Å from the Nϵ2 atom of His110, while one O atom is at 2.60 Å from the Tyr48 hydroxyl and the other O atom is at 2.83 Å from the Nϵ1 atom of Trp111, making H-bonds in all cases (Figure 3).

These H-bonds anchor the hydantoin moiety firmly in the anion binding site. Furthermore, the difference map shows a well-resolved density peak along a straight line between the N1′ (inhibitor) and Nϵ2His110, virtually equidistant from both N atoms (Figure 3). This peak attributed to an H atom clearly indicates a hydrogen bond. It also shows at least partial protonation of Nδ1His110. The position close to this atom but opposite the binding site, normally fully occupied by a water molecule, is partially occupied by a water molecule and

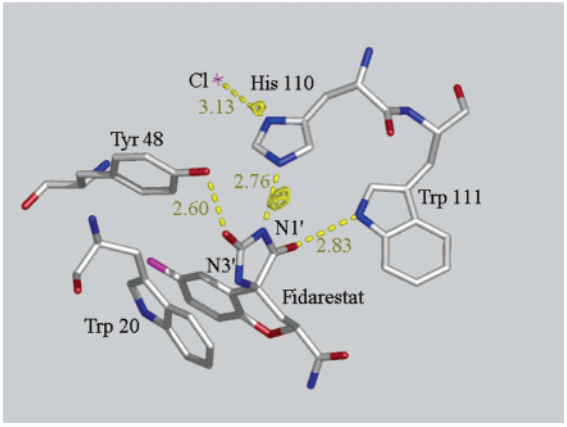

Figure 3. Diagram showing the interactions of fidarestat and the active site residues. Hydrogen bonds are given as dashed lines with distances in Å. The $F_o - F_c$ map (contoured at 2.0σ) shows the hydrogen atoms.

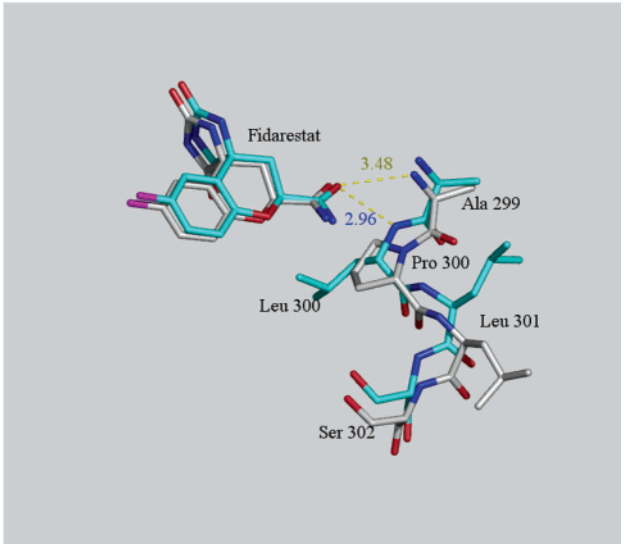

Figure 4. Superposition of the wild-type ALR2 (cyan carbons) and Leu-Pro mutant (gray carbons) residues 299−302 and fidarestat. Contacts of fidarestat with Leu300 (wild type) and Ala299 (Leu-Pro mutant) are shown as dashed lines with distances given in Å.

partially by a chloride ion, as indicated by anomalous scattering. This fact confirms the mechanism proposed by El-Kabbani et al.[24] that the binding of fidarestat involves a proton transfer from the inhibitor to His110. The fact that hydantoins are effective in vivo suggests that they pass the membrane barriers in their neutral form, and therefore, their binding is likely to be accompanied by that of a negative ion, as suggested by the crystal structure. The hydrogen connected to N3′ of the inhibitor points toward the aromatic plane of Trp20, suggesting an interaction with its π electrons (Figure 3).

At the level of Pro300, the mutation Leu-Pro causes a local shift of residues 299−302 (Figure 4), probably due to the need to accommodate the geometry of the proline main chain. The H-bond of the O atom of the fidarestat amide with the N atom of Leu300 in the wild-type (2.96 Å) is lost. There is a contact of 3.48 Å between the O atom of the fidarestat's exocyclic amide and the main chain N atom of Ala299, but the geometry is not adequate for a proper H-bond. The *B* factors of the N

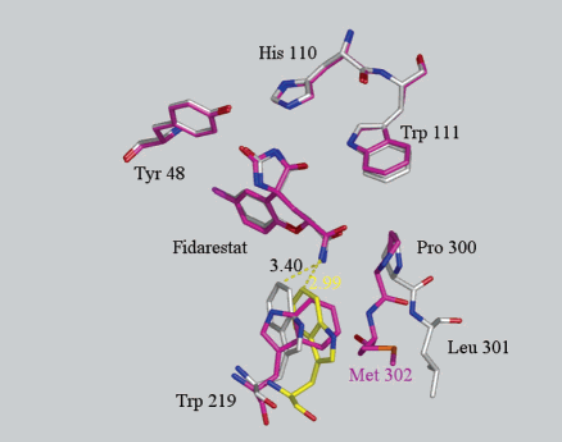

Figure 5. Superposition of the structure of the Leu300Pro ALR2−fidarestat (gray carbons) complex with the porcine ALR1−fidarestat complex (magenta carbons, minor conformation of Trp220 in yellow carbons) in the active site region.

and O atoms of the fidarestat's exocyclic amide group are larger than those of the remaining part of the inhibitor (∼14 vs ∼9 Å^2), suggesting that upon loss of the H-bond to Leu300 this portion gains higher residual mobility. In comparison, the *B* factors for these atoms in the fidarestat−ALR2 complex are of the same order as for the remaining portion of the inhibitor. The N atom of the amide group forms H-bonds to neighboring water molecules, while the O atom points to the protein but does not form any H-bonds.

Comparison with the ALR1−Fidarestat Complex. The superposition of the structure of the Leu300Pro hALR2−fidarestat complex with the porcine ALR1−fidarestat complex[28] in the active site region (Figure 5) gives rise to the following observations. The orientation of the inhibitor is very similar in both cases and the interactions of the hydantoin head with residues His110, Tyr48, and Trp111 follow the same patterns. The position of Pro300 in ALR2 superimposes with that of Pro301 in ALR1. In both cases the exocyclic amide moiety of the inhibitor does not form any H-bonds with the protein. Instead, close van der Waals contacts are observed. However, they are experienced through different contacting atoms in ALR1 and ALR2 because the flanking side chains of Pro300 (Pro301 in ALR1) and Trp219 (Trp220 in ALR1) reside on the protein backbones that take a slightly different trace in space because of structural and sequential differences. In the case of ALR1,[28] as indicated by the electron density map, the side chain of Trp220 occupies two conformations of which the minor one (20% occupancy) has an orientation similar to that observed in the ALR2 structure. The exocyclic amide moiety makes van der Waals contacts with the side chain of Trp220 in both conformations (2.99 Å for the minor and 3.59 Å for the major one). Because this side chain is already disordered in the aldehyde reductase holoenzyme,[13] this suggests that the short contact with the minor conformation might favor the major one.

Microcalorimetry. Comparison with Sorbinil. To trace the selectivity-determining features in terms of the thermodynamic data, we studied the binding of the related inhibitors fidarestat and sorbinil by microcalorimetry, toward wild-type aldose reductase and its Leu300Pro mutant. The only difference between these inhibitors is the exocyclic amide present in fidarestat.[12,15,24] The binding of the two inhibitors is affected by superimposed changes in protonation states that, in principle, have to be corrected before a subsequent factorization into absolute enthalpic and entropic contributions can be performed. However, assuming that for each individual ligand such protonation effects are identical for wild-type and mutant, a relative comparison of the thermodynamic differences and thus driving forces can be attempted for each ligand with respect to the wild-type and Leu300Pro mutant.

As shown in Table 1, the Gibbs free energy of binding $\Delta G°$ of fidarestat to wild-type is approximately 8 kJ/mol lower than that of fidarestat to Leu300Pro mutant. Fidarestat forms a hydrogen bond via its carbonyl oxygen of the exocyclic amide functional group and the Leu300 backbone NH. In the Leu300Pro ALR2−fidarestat complex a similar hydrogen bond cannot be formed because of the absence of an NH functionality in proline. Obviously this loss of a hydrogen bond relates to a $\Delta G°$ difference of ∼8 kJ/mol. In the case of the structurally related sorbinil, virtually identical $\Delta G°$ values are observed for the same pair. Because sorbinil lacks an appropriate functional group to hydrogen-bond to the main chain atoms of Leu300,[12] the loss of such functionality on the side of the protein due to the Leu300Pro replacement is not experienced by ligand binding. Interestingly enough, the free energy drop of fidarestat is mainly attributed to an enthalpy loss whereas entropy remains nearly unchanged. For sorbinil the unchanged $\Delta G°$ for both complexes factorizes into mutually compensating enthalpy and entropy changes leading to an enthalpically more favorable and entropically less beneficial binding to the wild-type. This thermodynamic difference possibly results from the presence of an interstitial water molecule mediating H-bonds between sorbinil and the main chain N atom of Leu300, similar to the one observed in the complex structure of sorbinil with pig lens aldose reductase (Figure 6). This water-

Table 1. ITC Measurements of the Binding of Fidarestat and Sorbinil to Leu300Pro Mutant and Wild-Type ALR2[a]

	K (10^6 L/mol)	std dev (10^6 L/mol)	$\Delta G°$ (kJ/mol)	$\Delta H°$ (kJ/mol)	std dev (kJ/mol)	$-T\Delta S°$ (kJ/mol)
			Fidarestat			
hALR2 WT	153.0	36.6	−46.7	−75.5	0.4	28.8
Leu300Pro	6.5	1.7	−38.9	−68.6	1.4	29.7
			Sorbinil			
hALR2 WT	4.5	0.6	−37.9	−51.8	0.8	13.9
Leu300Pro	6.1	0.1	−38.7	−46.7	0.7	8.0

[a] Studies reported so far for the binding of fidarestat and sorbinil to hALR2 concern IC_{50} measurements.[36−38] However, it should be noted that IC_{50} measurements can vary according to enzyme concentration, substrate, substrate concentrations, cofactor concentrations, reaction velocity, and other variables. Therefore, IC_{50} measurements are only indicative of binding constants obtained from calorimetric studies and are not directly comparable.

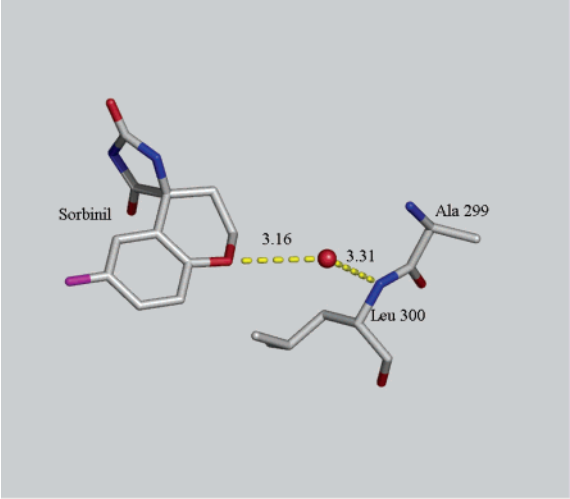

Figure 6. Diagram of the porcine ALR2−sorbinil complex showing the interstitial water molecule between sorbinil and the main chain N atom of Leu300.

mediated contact cannot exist in the mutant Leu300Pro. The sorbinil binding process to the wild-type captures, besides the ligand itself, a water molecule. The latter fact is assumed to be entropically unfavorable (in the present case a value for $-T\Delta S$ of approximately 6 kJ/mol is observed). For the mutant no interstitial water is arrested; accordingly, no entropic penalty has to be paid. On the other hand, sorbinil forms via its endocyclic ether function an H-bond to the interstitial water molecule in the wild-type, whereas a similar polar contact is missing in the mutant. In consequence, the inventory of polar contacts in solution versus protein remains uncompensated for the latter, which correlates, as indicated by experiment, with a less favorable enthalpic contribution ($\Delta H \approx 5$ kJ/mol).

Origin for Selectivity-Determining Features for Fidarestat Binding toward Aldose and Aldehyde Reductase. As shown in Table 1, the selectivity advantage (expressed as a ratio of the binding constants) of fidarestat to the Leu300Pro mutant over the wild-type is approximately 23-fold, arising from a $\Delta G°$ of 7.8 kJ/mol. This corresponds essentially to the enthalpy loss of one H-bond. However, considering the IC_{50} values for the binding of fidarestat to human ALR2 (9 nM) and porcine ALR1 (2500 nM), a larger difference (278-fold) in favor of ALR2 is indicated.[28] Even when IC_{50} values are only indicative of binding constants, this suggests that the binding of fidarestat toward both enzymes is discriminated by additional features, such as the difference attributed to the observed disorder of Trp220 in the ALR1 complex.[28] In the ALR2 mutant case, this residue is well ordered and makes a favorable contact (3.40 Å) with fidarestat. In the ALR1−fidarestat complex, this residue adopts at least two conformations, one with a shorter contact to fidarestat (2.99 Å) and one with a longer one (3.59 Å). Therefore, the favorable contact present in the ALR2−mutant case is lost, and a short contact appears, possibly leading to an enthalpic loss in the binding energy. Furthermore, Trp220 is already disordered in the aldehyde reductase holoenzyme,[13] which implies that there is no entropic gain associated with this residue when fidarestat is bound. Therefore, it is likely that this interaction of fidarestat with Trp 220 in ALR1, together with the loss of one H-bond, is responsible for the reduced free energy of binding accounting for the selectivity advantage.

Conclusions

The complex structure of the ALR2 mutant with fidarestat clearly shows that the H-bond of the exocyclic amide group of the inhibitor with Leu300 is lost without being compensated by a similar interaction. The thermodynamic data support this hypothesis because the predominant difference between mutant and wild-type is of an enthalpic nature. Facing the mutant data with the structure of the ALR1−fidarestat complex suggests that the H-bond toward Leu300 is a key determinant for the specificity of fidarestat for ALR2 over ALR1. Furthermore, the mutant complex indicates an additional selectivity-determining feature attributed to the split conformation of Trp220 observed in the ALR1 complex. Elucidation of such features on a molecular level and factorizing their contributions into enthalpic and entropic portions to binding are essential to provide the necessary guidelines for a rational lead optimization. With such information at hand, the medicinal chemist knows by which molecular properties his lead structures have to be equipped to achieve the desired selectivity advantage for a particular member of a protein family. High selectivity, e.g., avoiding unwanted cross-reactivity at other targets, is one major prerequisite for the development of safe drugs for the future.

Materials and Methods

Wild-Type ALR2 Expression and Purification. The open reading frame of the human aldose reductase gene (accession GenBank/EMBL data bank number J05017) was amplified by PCR from cDNA.[29] Cloned into the T7 RNA polymerase-based vector pET15b (Novagen), the protein was expressed in the *E. coli* strain BL21(DE3) (Novagen) induced by IPTG (Euromedex). After 3 h of incubation at 310 K, the pellet from a 4 L culture was disrupted by sonication and centrifuged. The supernatant was loaded onto a Talon metal-affinity column (Clontech). After thrombin cleavage of the hexahistidine extension, the protein was finally loaded onto a DEAE-Sephadex A-50 column (Pharmacia) and eluted with a NaCl gradient.

Leu300Pro ALR2 Expression and Purification. The mutation of the leucine 300 into proline was introduced by PCR, using the Pfu enzyme as polymerase to amplify the entire plasmid. After 25 cycles of PCR, the initial plasmid was digested by DpnI enzyme. After amplification (in DH5α *E. coli* strain), purification (with Nucleospin kit), and sequencing to confirm the mutation, the mutated plasmid was integrated in *E. coli* strain BL21(DE3) (Novagen) for production. The mutated protein was then expressed and purified by the same procedures as that used to obtain the wild-type protein.

Crystallization. Crystals of the Leu300Pro ALR2 holoenzyme−fidarestat ternary complex were grown in a Linbro 24-well culture plate (Flow Laboratories) using the vapor diffusion method.[30] Protein was cocrystallized with $NADP^+$ (Sigma) and inhibitor (in a 1:2:2 ratio of protein/coenzyme/inhibitor) in an equal volume of 50 mM ammonium citrate buffer (pH 5, containing 15% PEG 6000), previously equilibrated with 100-times diluted stock seed solutions. The 10 μL hanging drops were incubated at room temperature over a well solution of 20% PEG 6000 in 120 mM ammonium citrate. Crystals were transferred into a stabilization solution (25% PEG 6000) and then into a cryoprotecting solution (40% PEG 6000) and finally flash-frozen in either liquid nitrogen or ethane.

Data Collection and Processing. One crystal (with the dimensions of 0.6 mm × 0.4 mm × 0.3 mm) was used in the diffraction experiments. Almost complete synchrotron data sets

Table 2. Data Collection, Refinement, and Model Statistics for the Aldose Reductase Leu300Pro−Fidarestat Complex

parameters	
no. of crystals used	1
wavelength (Å)	0.652 55
space group	$P2_1$
unit-cell parameters	
a, b, c (Å)	49.118, 66.724, 47.092
α, β, γ (deg)	90.000, 92.787, 90.000
diffraction data	
resolution range (Å)	50.0−1.0
unique reflections	163 149
$R(I)_{sym}$ (%)	5.7
$R(I)_{sym}$ (%) (last shell 1.04−1)	38.6
completeness (%) (all)	99.8
completeness (%) (1.04−1.00)	100.0
$I/\sigma(I)$ (all)	18.5
$I/\sigma(I)$ (1.04−1.00)	3.51
refinement	
resolution range	10.0−1.0
size R_{free} set (%)	5
no. reflections	162 934
reflections (work/test)	154785/8149
R_{cryst}/R_{free} with H (%)	10.43/12.78
reflections with $F > 4\sigma_F$	
reflections (work/test)	129516/6769
R_{cryst}/R_{free} with H (%)	8.79/11.1
refinement with all reflections (50−1.0 Å)	
resolution range	50−1.0 Å
no. reflections	163 062
R_{cryst} with H (%)	10.6
R_{cryst} without H (%)	12.9
model	
protein residues (mean B factor, Å^2)	316 (8.6)
coenzyme molecules (mean B factor, Å^2)	1 (4.3)
inhibitor molecules (mean B factor, Å^2)	1 (6.0)
water molecules (mean B factor, Å^2)	588 (27.5)
bonds, rmsd (Å)	0.014
angle, rmsd (deg)	2.5
no. of double conformations (protein)	98
no. of water molecules with partial occupation	78
Ramachandran plot, most favored (%)	90.3
Ramachandran plot, allowed (%)	9.7

were collected at the APS (Argonne, IL) X-ray beamline 19ID of SBC-CAT (wavelength of 0.900 42 Å). Data from the crystals were reduced and scaled with HKL2000.[31] The ternary complex crystallized in the space group $P2_1$ with unit cell parameters $a = 49.118$ Å, $b = 66.724$ Å, $c = 47.092$ Å, $\alpha = 90.0°$, $\beta = 92.7°$, and $\gamma = 90.0°$. There was one monomeric unit per asymmetric cell, with a resolution range of 1.0−50 Å and 163 149 unique reflections. Data collecting and processing statistics are shown in Table 2.

Structure Refinement. The initial steps of the refinement were done using the CNS program[32] involving repeated cycles of conjugate gradient energy minimization, simulated annealing, and temperature factor refinement. The SHELXL program[33] package was used to carry out anisotropic conjugate gradient refinement, with H-atoms being introduced in the final cycles. The program XtalView/Xfit[34] was used to fit the amino acid side chains into the $2F_o - F_c$ and $F_o - F_c$ electron density maps. Water molecules were located in a difference map. Refinement data are shown in Table 2.

Isothermal Titration Calorimetry. Calorimetric measurements[35] were carried out using a MCS ITC instrument from MicroCal Inc. (Northampton). Human aldose reductase (ALR2) was expressed in *E. coli* and purified as described before. In each experiment, the ligand was titrated into the protein solution present in the 1.4 mL sample cell. The reference cell contained 0.1 mM sodium azide dissolved in demineralized water. All measurements were carried out at 298 K. The protein was dissolved in 10 mM Hepes buffer (pH 8) to concentrations of 18.9 and 37.8 μM for ALR2 wild-type enzyme and Leu300Pro mutant, respectively. The protein concentration was determined by UV spectroscopy (280 nm). The ligand solution contained 252 μM of the corresponding inhibitor, dissolved in the same buffer, with sonication to facilitate dissolution if necessary. The protein solution was saturated with an excess of $NADP^+$, which was also present in the ligand solution to the same concentration to avoid heat release caused by the dilution of the cofactor. Solutions were degassed at 293 K under vacuum for 10 min. At the commencement of the experiment, the protein solution in the sample cell was stirred at 400 rpm until a stable baseline had been achieved before the titration was initiated. The injection sequence started with an initial injection of 1.5 μL (for preventing diffusion effects arising from the experimental setup, not used in data fitting) followed by injections of 10 μL at intervals of 300 s until complete saturation was obtained. The heat caused by each inhibitor injection was obtained by integrating the calorimetric signal. Data were analyzed using the ORIGIN software (MicroCal Inc.) for fitting the data points to a single-site binding model that is in agreement with the results from X-ray crystallography.

Experimental heats of the protein−inhibitor titration were corrected for the heats of dilution by subtracting the corresponding data from a blank titration (inhibitor injected into buffer) or by subtracting the average of the last three data points obtained from the protein−inhibitor titration after saturation of the protein binding sites had been achieved. Both corrections resulted in approximately the same results. All measurements have been carried out at least in duplicate. With energy values, binding constants, and standard deviations derived from data fitting and subsequent average formation of the corresponding measurements, Gibbs free energy values and $-T\Delta S°$ were calculated using

$$\Delta G° = -RT \ln K_b = \Delta H° - T\Delta S°$$

where $R = 8.3144$ J/(mol K) and K_b is the binding constant.

The atomic coordinates are deposited with the Protein Data Bank and will be released immediately upon publication.

Acknowledgment. This work was supported by the Australian Research Council, Sanwa Kagaku Kenkyusyo Company, Ltd., the Centre National de la Recherche Scientifique (CNRS), the collaboration of Ecos Sud, the Institut National de la Santé et de la Recherche Médicale (INSERM), and the Hôpital Universitaire de Strasbourg (H.U.S), and a joint CNRS/DFG grant in the framework of the CERC3 project (Grant KL1204/4) and in part supported by the U.S. Department of Energy, Office of Energy Research, under Contract No. W-31-109-ENG-38. H.S. and G.K. thank the DFG for financial support (Grant KL1204/3).

References

(1) Jez, J. M.; Bennett, M. J.; Schlegel, B. P.; Lewis, M.; Penning, T. M. Comparative anatomy of the aldo−keto reductase superfamily. *Biochem. J.* **1997**, *326*, 625−636.
(2) Warren, J. C.; Murdock, G. L.; Ma, Y.; Goodman, S. R.; Zimmer, W. E. Molecular cloning of testicular 20α-hydroxysteroid dehydrogenase: identity with aldose reductase. *Biochemistry* **1993**, *32*, 1401−1406.
(3) Dunlop, M. Aldose reductase and the role of the polyol pathway in diabetic nephropathy. *Kidney Int.-Suppl.* **2000**, *77*, S3−S12.
(4) Kinoshita, J. H.; Nishimura, C. The involvement of aldose reductase in diabetic complications. *Diabetes Metab. Rev.* **1988**, *4*, 323−337.
(5) Yabe-Nishimura, C. Aldose reductase in glucose toxicity: a potential target for the prevention of diabetic complications. *Pharmacol. Rev.* **1998**, *50*, 21−33.
(6) Costantino, L.; Rastelli, G.; Gamberini, M. C.; Barlocco, D. Pharmacological approaches to the treatment of diabetic complications. *Expert Opin. Ther. Pat.* **2000**, *10*, 1245−1262.
(7) Oates, P. J.; Mylari, B. L. Aldose reductase inhibitors: therapeutic implications for diabetic complications. *Expert Opin. Invest. Drugs* **1999**, *8*, 1−25.
(8) Pfeifer, M. A.; Schumer, M. P.; Gelber, D. A. Aldose reductase inhibitors: the end of an era or the need for different trial design. *Diabetes* **1997**, *46*, S82−S89.
(9) Miyamoto, S. Recent advances in aldose reductase inhibitors: potential agents for the treatment of diabetic complications. *Expert Opin. Ther. Pat.* **2002**, *12*, 621−631.
(10) Sato, S.; Kador, P. F. Inhibition of aldehyde reductase by aldose reductase inhibitors. *Biochem. Pharmacol.* **1990**, *40*, 1033−1042.

(11) Ratliff, D. M.; Van der Jagt, D. J.; Eaton, R. P.; Van der Jagt, D. L. Increased levels of methylglyoxal-metabolizing enzymes in mononuclear cells from insulin-dependent diabetic patients with diabetic complications: aldose reductase, glyoxase I, and glyoxalase II. A clinical research center study. *J. Clin. Endocrinol. Metab.* **1996**, *81*, 488−492.
(12) Urzhumtsev, A.; Tête-Favier, F.; Mitschler, A.; Barbanton, J.; Barth, P.; Urzhumtseva, L.; Biellmann, J.-F.; Podjarny, A. D.; Moras, D. A. "Specificity" pocket inferred from the crystal structures of the complexes of aldose reductase with the pharmaceutically important inhibitors tolrestat and sorbinil. *Structure* **1997**, *5*, 601−612.
(13) El-Kabbani, O.; Judge, K.; Ginell, S. L.; Myles, D. A.; DeLucas, L. J.; Flynn, T. G. Structure of porcine aldehyde reductase holoenzyme. *Nat. Struct. Biol.* **1995**, *2*, 687−692.
(14) Da Settimo, F.; Primofiore, G.; Da Settimo, A.; La Motta, C.; Taliani, S.; Simorini, F.; Novellino, E.; Greco, G.; Lavecchia, A.; Boldrini, E. [1,2,4]Triazino[4,3-*a*]benzimidazole acetic acid derivatives: A new class of selective aldose reductase inhibitors. *J. Med. Chem.* **2001**, *44*, 4359−4369.
(15) Oka, M.; Matsumoto, Y.; Sugiyama, S.; Tsuruta, N.; Matsushima, M. A potent aldose reductase inhibitor, (2*S*,4*S*)-6-fluoro-2′,5′-dioxyspiro[chroman-4,4′-imidazoline]-2-carboxamide (fidarestat): Its absolute configuration and interaction with aldose reductase by X-ray crystallography. *J. Med. Chem.* **2000**, *43*, 2479−2483.
(16) Kurono, M.; Fujiwara, I.; Yoshida, K. Stereospecific interaction of a novel spirosuccinimide type aldose reductase inhibitor, AS-3201, with aldose reductase. *Biochemistry* **2001**, *40*, 8216−8226.
(17) Sarges, R.; Oates, P. J. Aldose reductase inhibitors: Recent developments. *Prog. Drug Res.* **1993**, *40*, 99−161.
(18) Eggler, J. F.; Larson, E. R.; Lipinski, C. A.; Mylari, B. L.; Urban, F. J. A perspective of aldose reductase inhibitors. In *Advances in Medicinal Chemistry*; Jai Press: Greenwich, CT, 1993; Vol. 2, pp 197−246.
(19) Larson, E. R.; Lipinski, C. A.; Sarges, R. Medicinal chemistry of aldose reductase inhibitors. *Med. Chem.* Rev. **1988**, *8*, 159−186.
(20) El-Kabbani, O.; Carper, D. A.; McGowan, M. H.; Devedjiev, Y.; Rees-Milton, K. J.; Flynn, T. G. Studies on the inhibitor-binding site of porcine aldehyde reductase: crystal structure of the holoenzyme−inhibitor ternary complex. *Proteins: Struct., Funct., Genet.* **1997**, *29*, 186−192.
(21) El-Kabbani, O.; Old, S. E.; Ginell, S. L.; Carper, D. A. Aldose and aldehyde reductases: structure−function studies on the coenzyme and inhibitor-binding sites. *Mol. Vision* **1999**, *5*, 20−26.
(22) Barski, O. A.; Gabbay, K. H.; Bohren, K. M. The C-terminal loop of aldehyde reductase determines the substrate and inhibitor specificity. *Biochemistry* **1996**, *35*, 14276−14280.
(23) El-Kabbani, O.; Rogniaux, H.; Barth, P.; Chung, R.; Fletcher, E.; Dorsselaer, A.; Podjarny, A. Aldose and aldehyde reductases: correlation of molecular modeling and mass spectrometric studies on the binding of inhibitors to the active site. *Proteins: Struct.. Funct.. Genet.* **2000**, *41*, 407−414.
(24) El-Kabbani, O.; Darmanin, C.; Schneider, T. R.; Hazemann, I.; Ruiz, F.; Oka, M.; Joachimiak, A.; Schulze-Briese, C.; Tomizaki, T.; Mitschler, A.; Podjarny, A. Ultra high-resolution structures of human aldose reductase holoenzyme complexed with fidarestat and minalrestat: Implications for the binding of cyclic imide inhibitors. *Proteins* **2004**, *55*, 805−813.
(25) El-Kabbani, O.; Darmanin, C.; Oka, M.; Schulze-Briese, C.; Tomizaki, T.; Hazemann, I.; Mitschler, A.; Podjarny, A. High resolution structures of human aldose reductase holoenzyme in complex with stereoisomers of the potent inhibitor fidarestat: Stereospecific interaction between the enzyme and a cyclic imide inhibitor. *J. Med. Chem.* **2004**, *47*, 4530−4537.
(26) Laskowski, R. A.; MacArthur, M. W.; Moss, D. S.; Thornton, J. M. PROCHECK: a program to check the stereochemical quality of protein structures. *J. Appl. Crystallogr.* **1993**, *26*, 283−291.
(27) Howard, E. I.; Sanishvili, R.; Cachau, R. E.; Mitschler, A.; Chevrier, B.; Barth, P.; Lamour, V.; Van Zandt, M.; Sibley, E.; Bon, C.; Moras, D.; Schneider, T. R.; Joachimiak, A.; Podjarny, A. Ultrahigh resolution drug design I: details of interactions in human aldose reductase−inhibitor complex at 0.66 Å. *Proteins* **2004**, *55*, 792−804.
(28) El-Kabbani, O.; Carbone, V.; Darmanin, C.; Oka, M.; Mitschler, A.; Podjarny, A.; Schulze-Briese, C.; Chung, R. P.-T. Structure of aldehyde reductase holoenzyme in complex with the potent aldose reductase inhibitor fidarestat: Implications for Inhibitor binding and selectivity. *J. Med. Chem.*, in press.
(29) Chung, S.; La Mendola, J. Cloning and sequence determination of human placental aldose reductase gene. *J. Biol. Chem.* **1989**, *264*, 4775−4777.
(30) McPherson, A. Crystallization of macromolecules: general principles. *Methods Enzymol.* **1985**, *114*, 112−120.
(31) Otwinowski, Z.; Minor, W. Processing of X-ray diffraction data collected in oscillation mode. *Methods Enzymol*. **1997**, *276*, 307−326.
(32) Navaza, J. Amore, an automated package for molecular refinement. *Acta Crystallogr., Sect. A* **1994**, *50*, 157−163.
(33) Sheldrick, G.; Schneider, T. SHELXL: high-resolution refinement. *Methods Enzymol.* **1997**, *277*, 319−343.
(34) McRee, D. E. XtalView/Xfit. A versatile program for manipulating atomic coordinates and electron density. *J. Struct. Biol.* **1999**, *125*, 156−165.
(35) Holdgate, G. A. Making cool drugs hot: Isothermal titration calorimetry as a tool to study binding energetics. *BioTechniques* **2001**, *31*, 164−184.
(36) Barski, O. A.; Gabbay, K. H.; Grimshaw, C. E.; Bohren, K. M. Mechanism of human aldose reductase: characterization of the active site pocket. *Biochemistry* **1995**, *34*, 11264−11275
(37) Mizuno, K.; Yamaguchi, T.; Unoue, A.; Tomiya, N.; Unno, R.; Miura, K.; Usui, T.; Matsumoto, Y.; Kondo, Y.; Yoshina, S.; Kondo, Y.; Sato, M.; Matsubara, A.; Kato, N.; Nakano, K.; Shirai, M.; Inoue, T.; Awaya, J.; Asaeda, N.; Hayasaka, I.; Koide, M.; Hibi, C.; Ban, M.; Sawai, K.; Kurono, M. Profile of a new aldose reductase inhibitor (2*S*,4*S*)-6-Fluoro-2′,5′-dioxyspiro[chroman-4,4′-imidazoline]-2-carboxamide. *Excerpta Med.* **1990**, *913*, 89−96.
(38) Poulsom, R. Inhibition of aldose reductase from human retina. *Curr. Eye Res.* **1987**, *6*, 427−32.

JM050424+